

Microwave-controlled switching of continuous time-crystalline behavior in driven-dissipative Rydberg ensembles

Xiao Chen(陈宵), Yun-Hai Li(李云海), Sheng-Jun Yuan(袁声军)

Citation: Chin. Phys. B. 35, 083202 (2026). DOI: 10.1088/1674-1056/ae7a07
http://cpb.iphy.ac.cn; http://iopscience.iop.org/cpb

What follows is a list of articles you may be interested in

Co-optimization of linear gain and dynamic range for atomic superheterodyne receivers based on homodyne readout

Chuan Qu(瞿川), Dongqin Guo(郭东琴), Jian Zhang(张剑)
Chin. Phys. B. 35, 013202 (2026). DOI: 10.1088/1674-1056/ade8e9

Rydberg six-wave mixing spectrum under ionized environment variation

Yinglong Diao(刁赢龙), Haoliang Hu(胡浩亮), Xiaofei Li(李小飞), Zhibo Li(李治博), Feitong Zeng(曾非同), Yanbin Chen(陈焱斌), Shuhang You(游书航)
Chin. Phys. B. 35, 023201 (2026). DOI: 10.1088/1674-1056/adf318

Polarization impact on sensitivity of Rydberg atom-based microwave sensors

Minghao Cai(蔡明皓), Aomao Wei(魏奥贸), Shanshan Chen(陈珊珊), Yuming Huang(黄聿铭)
Chin. Phys. B. 34, 083201 (2025). DOI: 10.1088/1674-1056/add005 **Optimization**

Optimization strategies for operational parameters of Rydberg atom-based amplitude modulation receiver

Yuhao Wu(吴宇豪), Dongping Xiao(肖冬萍), Huaiqing Zhang(张淮清), Sheng Yan(阎晟)
Chin. Phys. B. 34, 013201 (2025). DOI: 10.1088/1674-1056/ad886a

Microwave field sensor based on cold cesium Rydberg three-photon electromagnetically induced spectroscopy

Yuan-Yuan Wu(吴圆圆), Yun-Hui He(何云辉), Yue-Chun Jiao(焦月春), Jian-Ming Zhao(赵建明)
Chin. Phys. B. 33, 113201 (2024). DOI: 10.1088/1674-1056/ad7579

SPECIAL TOPIC — Quantum frontiers with Rydberg atoms

Microwave-controlled switching of continuous time-crystalline behavior in driven-dissipative Rydberg ensembles

Xiao Chen(陈宵)[1], Yun-Hai Li(李云海)[2], and Sheng-Jun Yuan(袁声军)[1,2,†]

[1] *Key Laboratory of Artificial Micro- and Nano-structures of Ministry of Education and School of Physics and Technology, Wuhan University, Wuhan* 430072, *China*

[2] *Wuhan Institute of Quantum Technology, Wuhan* 430206, *China*

(Received 11 April 2026; revised manuscript received 27 May 2026; accepted manuscript online 9 June 2026)

We propose a microwave-controlled interaction switch for driven-dissipative Rydberg ensembles. Through microwave dressing, the effective interaction is continuously reshaped from a short-range form dominated by van der Waals coupling to a longer-range form with an enhanced dipole-exchange contribution. This switch drives stationary-to-oscillatory transitions in both macroscopic thermal gases and two-dimensional (2D) lattices. In the mean-field description of thermal gases, microwave-controlled interaction tuning induces a supercritical Hopf bifurcation from a steady state to a stable limit cycle, giving rise to dissipative continuous time-crystalline behavior. In 2D lattices, where spatial correlations become important, cumulant-expansion calculations show that the same switching mechanism remains effective beyond mean-field theory. Although correlations reduce the classical oscillatory region, they sustain a correlation-modified oscillatory regime and additionally generate an oscillatory regime absent in mean-field theory. These results show that the proposed switch provides a unified route to controlling dissipative oscillatory behavior from thermal Rydberg gases to 2D lattices.

Keywords: Rydberg atoms, continuous time crystal, microwave dressing, driven-dissipative systems

PACS: 32.80.Ee, 32.80.Qk, 05.70.Ln, 42.50.Nn

DOI: 10.1088/1674-1056/ae7a07 **CSTR:** 32038.14.CPB.ae7a07

1. Introduction

Spontaneous symmetry breaking provides a unifying framework for understanding the emergence of ordered phases in many-body systems.[1] Its extension to the temporal domain has stimulated broad interest in time crystals,[2,3] which are characterized by the spontaneous breaking of time-translation symmetry. Although continuous time crystals (CTCs) are ruled out in thermal equilibrium by general no-go theorems,[4,5] persistent oscillatory phases can emerge in nonequilibrium open systems through the interplay of coherent driving, dissipation, and interactions.[6–8] In these regimes, continuous time-crystalline behavior manifests as robust, long-lived oscillations of macroscopic observables in the absence of explicit periodic driving. Rydberg atomic systems provide a particularly attractive platform for exploring these nonequilibrium phases, owing to their strong interactions, long lifetimes, and a high degree of optical controllability.[9–12] Indeed, driven-dissipative Rydberg ensembles have been shown to support a rich variety of nonequilibrium phenomena, including multistability,[13–19] collective synchronization,[20] and continuous time crystals.[21–23]

In thermal Rydberg gases, dissipative continuous time-crystalline behavior has been observed and is commonly understood at the mean-field level, where limit-cycle dynamics arise from nonlinear interaction-induced feedback.[14,20–23] Meanwhile, theoretical studies of driven-dissipative two-dimensional (2D) lattices have shown that beyond-mean-field correlations can qualitatively reshape this picture.[24] Correlations can suppress part of the classical oscillatory region while also generating oscillatory regimes absent at the mean-field level. These advances have substantially deepened our understanding of dissipative continuous time-crystalline behavior in Rydberg systems.

However, most existing studies have focused primarily on the existence and characterization of oscillatory phases, whereas their controllable switching remains much less explored.[25] External tuning of the effective interaction may therefore provide a direct route to switching the system between stationary and oscillatory regimes. More broadly, optical and microwave control fields have become versatile tools for engineering light–matter interactions and tunable responses across atomic and photonic platforms.[26,27]

A direct way to achieve such interaction tuning is through microwave dressing of Rydberg states.[28] By coupling nearby Rydberg levels with opposite parities, a microwave field can modify both the strength and the spatial character of the effective interatomic interaction. Microwave dressing has been widely used for interaction engineering and state manipulation in Rydberg systems.[29–32] This makes it a natural can-

†Corresponding author. E-mail: s.yuan@whu.edu.cn

© 2026 Chinese Physical Society and IOP Publishing Ltd. All rights, including for text and data mining, AI training, and similar technologies, are reserved.

didate for realizing interaction-based switching between stationary and oscillatory regimes in driven-dissipative Rydberg ensembles.

In this work, we propose a microwave-controlled interaction switch for driven-dissipative Rydberg ensembles. The key idea is that the microwave mixing angle θ continuously reshapes the effective interaction from a short-range van der Waals form to a longer-range form with an enhanced dipole-exchange contribution, providing an experimentally tunable parameter for controlling the nonlinear feedback responsible for dissipative oscillations. We demonstrate this switch in two complementary settings. First, within the mean-field description of a macroscopic thermal gas, we show that microwave-induced interaction tuning drives a supercritical Hopf bifurcation[33] from a steady state to a stable limit cycle, giving rise to dissipative continuous time-crystalline behavior. Second, in a 2D lattice, where spatial correlations cannot be neglected, we show that the same switching mechanism remains effective beyond mean-field theory: correlations suppress part of the classical oscillatory region while still supporting a correlation-modified oscillatory regime and additionally enabling an oscillatory regime absent at the mean-field level. This establishes a direct link between microwave-controlled interaction engineering and nonequilibrium dynamical phases in driven-dissipative Rydberg systems, and provides a unified route to controlling dissipative oscillatory behavior from thermal gases to 2D lattices.

2. Physical model and methods

2.1. Model and effective Hamiltonian

We consider an ensemble of N interacting Rydberg atoms, as schematically illustrated in Fig. 1. Each atom is described by a ladder-type level structure consisting of a ground state $|g\rangle$, an intermediate excited state $|e\rangle$, and a Rydberg state $|r_1\rangle$. A probe laser with Rabi frequency Ω_p and detuning Δ_p drives the transition $|g\rangle \leftrightarrow |e\rangle$, while a control laser with Rabi frequency Ω_c couples $|e\rangle \leftrightarrow |r_1\rangle$. We define the atomic operators for the i-th atom as $\hat{\sigma}^{(i)}_{\alpha\beta} = |\alpha\rangle_i\langle\beta|$, where $\alpha,\beta \in \{g,e,r_1,r_2,\ldots\}$. Within the rotating-wave approximation, the single-particle Hamiltonian of the bare three-level system is written as

$$\hat{H}_\mathrm{single} = \sum_i \left(\Delta_\mathrm{p}\hat{\sigma}^{(i)}_{gg} + \Omega_\mathrm{p}\left(\hat{\sigma}^{(i)}_{eg} + \hat{\sigma}^{(i)}_{ge}\right) + \Omega_\mathrm{c}\left(\hat{\sigma}^{(i)}_{r_1e} + \hat{\sigma}^{(i)}_{er_1}\right)\right). \tag{1}$$

In the absence of microwave dressing, atoms excited to $|r_1\rangle$ interact via the van der Waals (vdW) potential[34]

$$\hat{H}_\mathrm{int} = \sum_{i<j} V_{11}(R_{ij})\,\hat{\sigma}^{(i)}_{r_1r_1}\hat{\sigma}^{(j)}_{r_1r_1}, \quad V_{11}(R_{ij}) = \frac{C_6}{R_{ij}^6}, \tag{2}$$

where R_{ij} denotes the distance between atoms i and j, and C_6 is the vdW interaction coefficient.

To engineer the interaction profile, we introduce a microwave field that couples $|r_1\rangle$ to a nearby Rydberg state $|r_2\rangle$ of opposite parity, with Rabi frequency Ω_m and detuning Δ_m. Diagonalizing the $\{|r_1\rangle, |r_2\rangle\}$ subspace yields the microwave-dressed states[35]

$$\begin{aligned} |+\rangle &= \cos\theta\,|r_1\rangle + \sin\theta\,|r_2\rangle, \\ |-\rangle &= -\sin\theta\,|r_1\rangle + \cos\theta\,|r_2\rangle, \end{aligned} \tag{3}$$

where the mixing angle satisfies $\tan(2\theta) = 2\Omega_\mathrm{m}/\Delta_\mathrm{m}$. The microwave field thus provides a direct control parameter θ for tuning the Rydberg character of the dressed states.

The control laser then couples $|e\rangle$ simultaneously to $|+\rangle$ and $|-\rangle$. When the microwave-induced Autler–Townes splitting is much larger than the remaining dynamical scales, the control field can be tuned into resonance with the $|e\rangle \leftrightarrow |+\rangle$ transition while remaining far detuned from $|-\rangle$. In this regime, the $|-\rangle$ state can be adiabatically eliminated, and the system reduces to an effective three-level ladder $\{|g\rangle, |e\rangle, |+\rangle\}$ (see Appendix A for details). The corresponding effective Rabi frequency is $\Omega_\mathrm{c}^{(\mathrm{eff})} = \Omega_\mathrm{c}\cos\theta$. To isolate the effect of interaction tuning from trivial changes in the driving strength, we assume that the control-laser intensity is adjusted together with θ such that $\Omega_\mathrm{c}^{(\mathrm{eff})}$ remains constant. In the following, this constant effective coupling is again denoted by Ω_c.

Projecting the interaction Hamiltonian onto the dressed $|+\rangle$ manifold yields the effective two-body interaction (see Appendix A for details)

$$U(R_{ij},\theta) = V_{11}(R_{ij}) + \frac{1}{2}\sin^2(2\theta)\big(V_{12}(R_{ij}) - V_{11}(R_{ij})\big), \tag{4}$$

where $V_{12}(R_{ij}) = C_3/R_{ij}^3$ denotes the dipole-dipole (dipole-exchange) interaction. The first term represents the vdW background, while the second term introduces a microwave-controlled longer-range component originating from the exchange process $|r_1r_2\rangle \leftrightarrow |r_2r_1\rangle$.[34] Therefore, increasing θ continuously reshapes the effective interaction from a vdW-dominated short-range form to a longer-range profile with an enhanced dipole-exchange contribution.

The resulting effective many-body Hamiltonian takes the form

$$\begin{aligned} \hat{H}_\mathrm{eff} = &\sum_i \left(\Delta_\mathrm{p}\hat{\sigma}^{(i)}_{gg} + \Omega_\mathrm{p}(\hat{\sigma}^{(i)}_{eg} + \hat{\sigma}^{(i)}_{ge}) + \Omega_\mathrm{c}(\hat{\sigma}^{(i)}_{+e} + \hat{\sigma}^{(i)}_{e+})\right) \\ &+ \sum_{i<j} U(R_{ij},\theta)\hat{\sigma}^{(i)}_{++}\hat{\sigma}^{(j)}_{++}. \end{aligned} \tag{5}$$

This formulation unifies the microwave-off case, $\theta = 0$, and the microwave-dressed case, $\theta \neq 0$, and identifies θ as the single external control parameter of the dynamical switching mechanism studied below.

Accounting for spontaneous emission from the intermediate state via the decay channel $|e\rangle \to |g\rangle$ with rate γ, the

open-system dynamics are governed by the Lindblad master equation[35]

$$\frac{\partial\hat{\rho}}{\partial t} = -i[\hat{H}_{\rm eff},\hat{\rho}] + \gamma\sum_i\left(\hat{\sigma}_{ge}^{(i)}\hat{\rho}\hat{\sigma}_{eg}^{(i)} - \frac{1}{2}\{\hat{\sigma}_{ee}^{(i)},\hat{\rho}\}\right), \quad (6)$$

where $\hat{\rho}$ is the many-body density matrix, and the anticommutator is defined as $\{\hat{A},\hat{B}\} = \hat{A}\hat{B} + \hat{B}\hat{A}$. The radiative decay of the Rydberg states is neglected throughout, assuming a parameter regime in which their lifetime is much longer than the timescale of the driven-dissipative dynamics considered here.

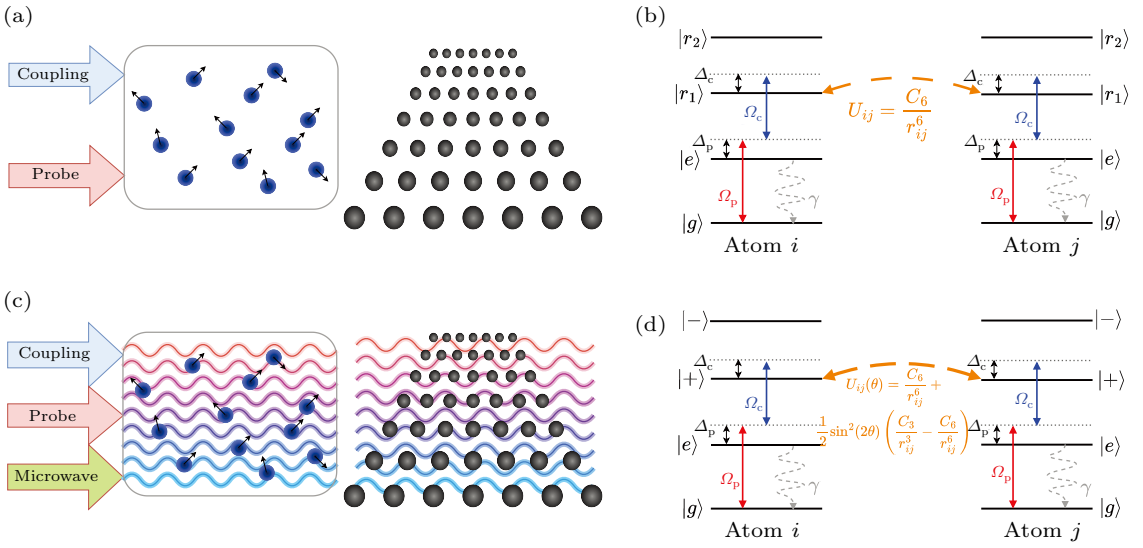


Fig. 1. Schematic illustration of the microwave-controlled dynamical switch in Rydberg thermal gases and 2D lattices. (a) and (c) Schematics of the system without and with microwave dressing, respectively. (b) and (d) Corresponding energy-level diagrams and interatomic interaction potentials for the two configurations.

2.2. Mean-field description for thermal gases

We first consider a macroscopic thermal Rydberg gas. In this limit, atomic motion tends to wash out spatial correlations, and the nonequilibrium dynamics can be described at the mean-field (MF) level. We accordingly factorize two-body expectation values as $\langle\hat{\sigma}_{\alpha\beta}^{(i)}\hat{\sigma}_{\mu\nu}^{(j)}\rangle = \langle\hat{\sigma}_{\alpha\beta}^{(i)}\rangle\langle\hat{\sigma}_{\mu\nu}^{(j)}\rangle$ for $i \neq j$,[36,37] and assume a homogeneous gas such that the single-particle expectation values are site-independent, i.e. $\rho_{\alpha\beta} \equiv \langle\hat{\sigma}_{\alpha\beta}^{(i)}\rangle$.

Within this approximation, the interaction enters only through a collective mean-field shift. We define the effective collective interaction strengths[24,38] $\chi_1 = \sum_{j\neq i}V_{11}(R_{ij})$ and $\chi_2 = \sum_{j\neq i}V_{12}(R_{ij})$ for the vdW and dipole-exchange contributions, respectively. In practice, these quantities are regarded as effective collective interaction parameters that absorb the density, geometry, and short-distance regularization of the macroscopic gas. The microwave-controlled collective interaction is then

$$\chi(\theta) = \chi_1 + \frac{1}{2}\sin^2(2\theta)(\chi_2 - \chi_1). \quad (7)$$

Thus, in the thermal-gas MF description, the many-body interaction reduces to a nonlinear density-dependent shift $\chi(\theta)\rho_{++}$ of the dressed Rydberg level. Changing the microwave mixing angle modifies this shift through $\chi(\theta)$ and thereby affects the existence and stability of the MF fixed points. Starting from the master equation, we obtain the following closed set of MF equations:

$$\begin{aligned}
\dot{\rho}_{gg} &= \mathrm{i}\Omega_{\rm p}(-\rho_{eg} + \rho_{ge}) + \gamma\rho_{ee},\\
\dot{\rho}_{ee} &= -\gamma\rho_{ee} - \mathrm{i}\left(\Omega_{\rm c}\rho_{+e} - \Omega_{\rm c}\rho_{e+} - \Omega_{\rm p}\rho_{eg} + \Omega_{\rm p}\rho_{ge}\right),\\
\dot{\rho}_{++} &= \mathrm{i}\Omega_{\rm c}(\rho_{+e} - \rho_{e+}),\\
\dot{\rho}_{ge} &= -\frac{\gamma\rho_{ge}}{2} - \mathrm{i}\left(\Delta_{\rm p}\rho_{ge} - \Omega_{\rm c}\rho_{g+} + \Omega_{\rm p}\rho_{ee} - \Omega_{\rm p}\rho_{gg}\right),\\
\dot{\rho}_{g+} &= \mathrm{i}\left(-\Delta_{\rm p}\rho_{g+} + \Omega_{\rm c}\rho_{ge} - \Omega_{\rm p}\rho_{e+} + \chi(\theta)\rho_{++}\rho_{g+}\right),\\
\dot{\rho}_{e+} &= -\frac{\gamma\rho_{e+}}{2} - \mathrm{i}\Big(\Omega_{\rm c}\rho_{++} - \Omega_{\rm c}\rho_{ee}\\
&\quad + \Omega_{\rm p}\rho_{g+} - \chi(\theta)\rho_{++}\rho_{e+}\Big).
\end{aligned} \quad (8)$$

These equations form the basis for the mean-field phase-diagram analysis and for identifying the onset of limit-cycle dynamics in the thermal-gas regime.

2.3. Cumulant expansion method for 2D lattices

We next consider a 2D square lattice, where atomic motion is frozen and spatial correlations can no longer be neglected. In this regime, the MF approximation is generally insufficient, and we instead employ a second-order cumulant expansion method (CME).[39–43]

Within the CME, we evolve both the single-particle expectation values $\langle\hat{\sigma}_{\mu\nu}^{(i)}\rangle$ and the two-body correlators $C_{\mu\nu,\alpha\beta}^{ij} = \langle\hat{\sigma}_{\mu\nu}^{(i)}\hat{\sigma}_{\alpha\beta}^{(j)}\rangle - \langle\hat{\sigma}_{\mu\nu}^{(i)}\rangle\langle\hat{\sigma}_{\alpha\beta}^{(j)}\rangle$. Because of the two-body interaction term in $\hat{H}_{\rm eff}$, the corresponding equations of motion are coupled to three-body expectation values. To close the hierarchy, we neglect three-body cumulants and approximate

$$\langle\hat{A}\hat{B}\hat{C}\rangle = \langle\hat{A}\rangle\langle\hat{B}\hat{C}\rangle + \langle\hat{B}\rangle\langle\hat{A}\hat{C}\rangle + \langle\hat{C}\rangle\langle\hat{A}\hat{B}\rangle - 2\langle\hat{A}\rangle\langle\hat{B}\rangle\langle\hat{C}\rangle. \quad (9)$$

This approximation retains all two-body correlations while discarding higher-order correlations.

A brute-force implementation would require $O(N^2)$ coupled equations for the two-body correlators. However, for a square lattice with periodic boundary conditions, translational invariance implies that all single-particle expectation values are site-independent, $\langle\hat{\sigma}_{\mu\nu}^{(i)}\rangle \equiv \rho_{\mu\nu}$, and that the two-body correlators depend only on the relative displacement, such that $C_{\mu\nu,\alpha\beta}^{ij} \equiv C_{\mu\nu,\alpha\beta}(\boldsymbol{r}_i - \boldsymbol{r}_j)$. This reduces the number of independent dynamical variables from $O(N^2)$ to $O(N)$, making long-time simulations of large lattices numerically feasible.

To compare the lattice calculations with the thermal-gas MF description on a common energy scale, we parameterize the microscopic interaction coefficients C_3 and C_6 in terms of the collective interaction strengths χ_1 and χ_2. For a square lattice with lattice constant a, we have

$$C_6 = \chi_1 \left(\sum_{j\neq i} \frac{1}{R_{ij}^6}\right)^{-1}, \qquad C_3 = \chi_2 \left(\sum_{j\neq i} \frac{1}{R_{ij}^3}\right)^{-1}. \quad (10)$$

This mapping provides a consistent way of matching the characteristic interaction scales of the two descriptions, allowing us to isolate the role of spatial correlations in the lattice dynamics.

3. Results and discussion

3.1. Microwave-controlled onset of dissipative oscillations in thermal gases

We first analyze the mean-field dynamical response of a macroscopic thermal gas and show that microwave dressing provides a direct control knob for switching oscillatory dynamics on and off. In the absence of microwave dressing ($\theta = 0$), the effective interaction is dominated by the short-range van der Waals contribution, and the $\Delta_\mathrm{p} - \Omega_\mathrm{p}$ phase diagram contains only steady-state solutions. By contrast, when the microwave field is applied and the mixing angle is tuned to $\theta = \pi/4$, the enhanced longer-range dipole-exchange contribution qualitatively modifies the nonlinear feedback in the mean-field equations. Linear-stability analysis then reveals three dynamical regimes in the $\Delta_\mathrm{p} - \Omega_\mathrm{p}$ plane, as shown in Fig. 2(a): a monostable region with a single stable fixed point, a bistable region with two coexisting stable fixed points, and an oscillatory region in which the stable fixed point loses stability and the long-time dynamics approach a limit cycle.[33] Specifically, we obtain the fixed points of the MF equations and determine their stability from the eigenvalues of the corresponding Jacobian matrix. The corresponding bifurcation diagram in Fig. 2(b) shows how the dressed-state population ρ_{++} evolves across these regimes as the probe detuning varies.

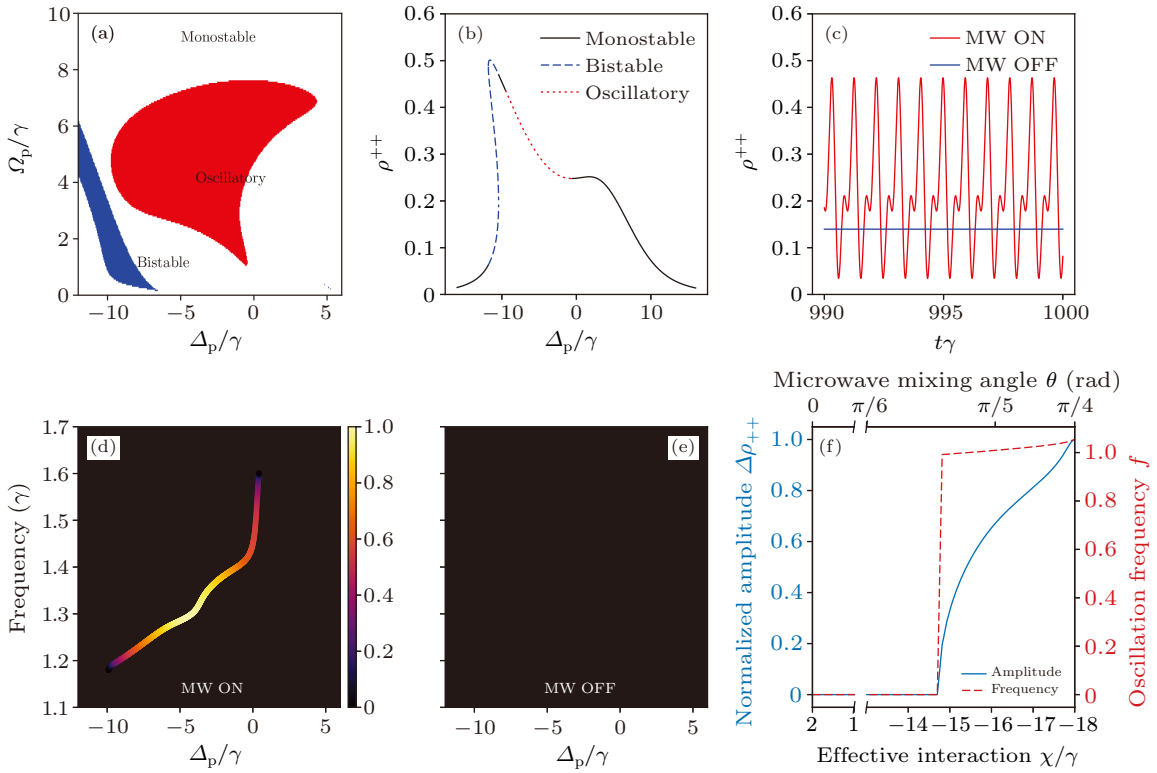


Fig. 2. Mean-field dynamics and microwave-controlled onset of oscillatory phases in thermal Rydberg gases. (a) Dynamical phase diagram in the $\Delta_\mathrm{p} - \Omega_\mathrm{p}$ plane for the microwave-dressed case ($\theta = \pi/4$), where the white, blue, and red regions denote the monostable, bistable, and oscillatory phases, respectively. (b) Bifurcation diagram of the dressed-state population ρ_{++} versus the probe detuning Δ_p at $\Omega_\mathrm{p} = 4\gamma$. (c) Late-time evolution of ρ_{++} for the microwave-on and microwave-off cases at $\Delta_\mathrm{p} = -2.4\gamma$ and $\Omega_\mathrm{p} = 2.1\gamma$. (d), (e) Oscillation frequency and normalized amplitude (color scale) of ρ_{++} as functions of Δ_p for the microwave-on and microwave-off cases, respectively, at $\Omega_\mathrm{p} = 5\gamma$. (f) Oscillation amplitude and frequency of ρ_{++} versus the collective interaction strength χ (bottom axis) and the corresponding microwave mixing angle θ (top axis) at $\Delta_\mathrm{p} = -2.4\gamma$ and $\Omega_\mathrm{p} = 2.1\gamma$. Other parameters are $\Omega_\mathrm{c} = 6\gamma$, $\chi_1 = 2\gamma$, $\chi_2 = -38\gamma$, and $\gamma = 1$.

Solid and dashed curves represent stable and unstable steady-state branches, respectively, while the dotted segment indicates the parameter window in which the attractor is a stable limit cycle. The switching behavior is illustrated more directly in Fig. 2(c), which shows the late-time evolution of ρ_{++} for a representative parameter point within the oscillatory region. In the microwave-off case, the system eventually relaxes to a steady state. When the microwave field is turned on, the dressed interaction drives the system into a stable limit cycle, leading to persistent oscillations.

We further test the robustness of the switch with respect to probe-detuning variations. Figures 2(d) and 2(e) compare the detuning dependence of the oscillation frequency and amplitude for the microwave-on and microwave-off cases at fixed $\Omega_{\rm p} = 5\gamma$. With microwave dressing, stable finite-frequency oscillations persist throughout an extended detuning window, whereas the microwave-off case relaxes to a steady state over the same range. Thus, the robustness of the switching effect is reflected directly in the finite-frequency oscillatory response of the microwave-on case and its absence in the microwave-off case. The frequency in Fig. 2(d) is extracted from the fundamental period of the long-time trajectory after transient dynamics have been discarded. In the scanned oscillatory interval, this period is determined from successive maxima of $\rho_{++}(t)$; possible higher harmonics associated with the non-sinusoidal waveform do not affect the fundamental frequency reported here.

The nature of the mean-field transition is clarified in Fig. 2(f), which shows the oscillation amplitude and frequency as functions of the collective interaction strength χ. At the critical point $\chi_{\rm c}$, a pair of complex-conjugate eigenvalues of the linearized dynamics crosses the imaginary axis, and the stable fixed point loses stability. The oscillation amplitude emerges continuously from zero with the characteristic scaling $\propto (\chi - \chi_{\rm c})^{1/2}$, while the oscillation frequency becomes finite at the onset. Together, these features identify the transition as a supercritical Hopf bifurcation.[33] Thus, in the mean-field description of a thermal gas, the proposed switch drives the system across the Hopf threshold, thereby switching the dynamics from a steady state to dissipative continuous time-crystalline behavior.

3.2. Correlation effects and microwave-controlled oscillatory regimes in 2D lattices

We now turn to the 2D lattice, where spatial correlations render a purely mean-field description insufficient. The key question is whether the proposed switch remains effective beyond mean-field theory and how correlations modify the oscillatory phase diagram. To address this, we compare the cumulant-expansion results with the corresponding mean-field results.

As in the thermal-gas case, no long-time oscillations are found for $\theta = 0$, so the lattice relaxes to a steady state throughout the parameter range considered. When the microwave field is turned on ($\theta = \pi/4$), however, the CME dynamics reveal two distinct correlation effects. First, correlations suppress part of the oscillatory region predicted by mean-field theory. This surviving oscillatory domain, which remains continuously connected to the mean-field oscillatory phase, is referred to as qCTC-I, following the terminology of Ref. [24]. Second, the CME additionally yields an oscillatory regime in a region where mean-field theory predicts only a steady state. We refer to this regime as qCTC-II, again following the same terminology, and interpret it here as a correlation-enabled oscillatory regime within the second-order CME description. For the CME amplitude maps, the oscillation amplitude is evaluated as half of the peak-to-peak variation of the long-time $\rho_{++}(t)$ trajectory, and parameter points with amplitudes below 10^{-6} are classified as stationary. The small-amplitude edge of qCTC-II should therefore be understood as an operational numerical boundary associated with its smooth onset rather than as a sharp mean-field-like instability line.

These effects are summarized in Fig. 3(a), where the CME oscillation amplitude is overlaid on the mean-field oscillatory region. The comparison shows that correlations do not simply suppress oscillations uniformly. Instead, they reshape the phase diagram in two qualitatively different ways: they suppress part of the classical oscillatory region but also enable oscillatory behavior in a distinct parameter window outside the mean-field boundary.

The representative late-time evolutions of ρ_{++} in Figs. 3(b)–3(e) make these two effects explicit. In the qCTC-I regime (Fig. 3(d)), both mean-field and CME approaches yield persistent oscillations when the microwave field is on, but the CME oscillation amplitude is significantly reduced. This indicates that spatial correlations modify, rather than eliminate, the classical limit-cycle dynamics. By contrast, for parameters well outside the oscillatory regime (Fig. 3(c)), both descriptions relax to a steady state. More interesting behavior occurs near the mean-field phase boundary. Figure 3(e) shows a point that lies inside the mean-field oscillatory region but outside qCTC-I: here, mean-field theory predicts a limit cycle, whereas the CME dynamics relax to a steady state, demonstrating that correlations can suppress the classical oscillatory order. Conversely, Fig. 3(b) shows the qCTC-II regime, where the mean-field solution is steady but the CME solution develops persistent oscillations. The oscillatory response therefore originates beyond the mean-field description and is enabled by spatial correlations captured at the two-body cumulant level. In the qCTC-I and qCTC-II regimes (Figs. 3(d) and 3(b)), turning off the microwave field switches the system back to a steady state, showing that the proposed switch remains effective in Rydberg 2D lattices.

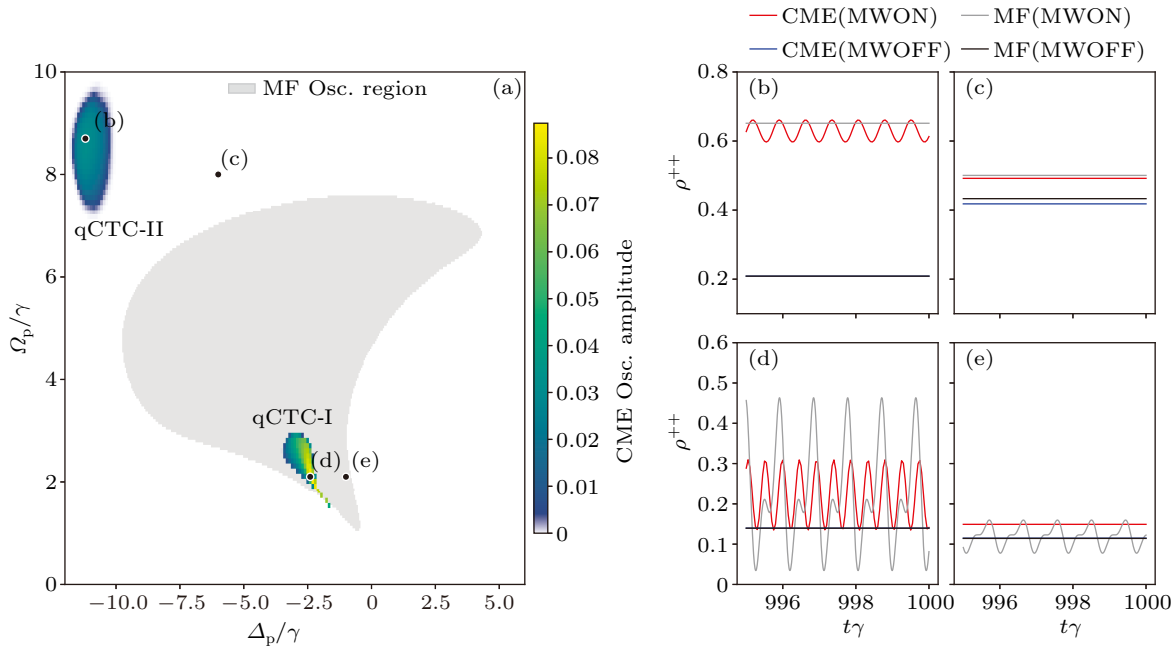


Fig. 3. Correlation-induced reshaping of the oscillatory phase diagram in a 2D lattice. (a) Dynamical phase diagram obtained from the cumulant expansion method (CME) for a 33×33 square lattice with microwave dressing ($\theta = \pi/4$). The color scale shows the oscillation amplitude of ρ_{++}, and the gray shaded area marks the oscillatory region predicted by mean-field (MF) theory. Following Ref. [24], we refer to the surviving oscillatory region inside the MF boundary as qCTC-I and the additional oscillatory regime outside the MF boundary as qCTC-II. (b)–(e) Late-time evolution of ρ_{++} for representative parameter points, comparing CME and MF results with and without microwave dressing: (b) qCTC-II regime ($\Delta_p = -11.2\gamma, \Omega_p = 8.7\gamma$); (c) stationary regime ($\Delta_p = -6.0\gamma, \Omega_p = 8.0\gamma$); (d) qCTC-I regime ($\Delta_p = -2.4\gamma, \Omega_p = 2.1\gamma$); (e) a point inside the MF oscillatory region but outside qCTC-I ($\Delta_p = -1.0\gamma, \Omega_p = 2.1\gamma$). Other parameters are the same as in Fig. 2.

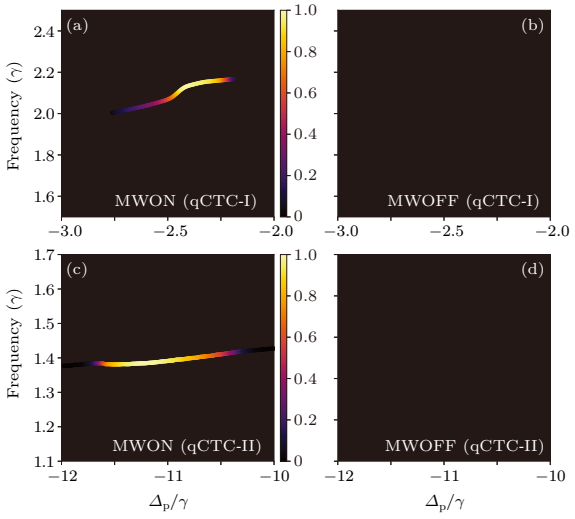


Fig. 4. Microwave-controlled frequency and amplitude response in the correlated lattice regime. (a) and (b) Oscillation frequency and normalized amplitude (color scale) of ρ_{++} versus Δ_p near the qCTC-I regime for the microwave-on and microwave-off cases, respectively, at $\Omega_p = 2.1\gamma$. (c) and (d) Corresponding responses near the qCTC-II regime at $\Omega_p = 8.7\gamma$. Other parameters are identical to those in Fig. 3.

Figure 4 further demonstrates the robustness of the proposed switch in the 2D lattice by comparing the detuning-dependent frequency and amplitude responses with and without microwave dressing near the qCTC-I and qCTC-II regimes. In both cases, microwave dressing produces a finite-frequency oscillatory response over a wide detuning interval, whereas no oscillations appear in the corresponding microwave-off case over the same range. This shows that the switching effect is not restricted to a fine-tuned point but remains robust against parameter variations even in the presence of many-body correlations.

To further benchmark the CME results, we have also performed a 2×2 cluster mean-field (CMF)[44] calculation for the same four representative parameter points shown in Fig. 3. The CMF treatment, which retains short-range correlations exactly within each cluster while approximating the inter-cluster coupling at the mean-field level, provides a complementary beyond-mean-field description. As shown in Appendix A, the CMF results qualitatively reproduce the same phase classification obtained from the CME analysis: persistent oscillations are found in the qCTC-I and qCTC-II regimes, whereas stationary behavior is recovered both at the reference stationary point and at the point lying inside the mean-field oscillatory region but outside qCTC-I. This agreement indicates that the correlation-induced suppression and emergence of oscillatory behavior identified here are not specific to the CME treatment alone, further supporting the robustness of the proposed switching mechanism beyond mean-field theory.

3.3. Distinguishing qCTC-I from qCTC-II

To better understand the difference between qCTC-I and qCTC-II, we analyze how the oscillatory response evolves as the collective interaction strength χ is increased, as shown in Fig. 5. This comparison reveals two qualitatively distinct onset behaviors.

For qCTC-I, the oscillatory phase remains continuously connected to the mean-field limit-cycle regime. As shown in Fig. 5(a), the oscillation amplitude of the single-particle observable ρ_{++} emerges from zero at a well-defined critical point χ_c, but its onset is modified relative to the mean-field square-root scaling. Within the CME, the initial growth is approximately linear in $\chi - \chi_c$, indicating that spatial correlations quantitatively modify the classical critical behavior. The oscillation frequency also becomes finite at the critical point χ_c. At the same time, the nearest-neighbor correlator $C^{01}_{++,++}$, shown in Fig. 5(b), appears together with the onset of macroscopic oscillations, signaling the buildup of spatial correlations at the transition. Deeper in the oscillatory regime, the correlator decreases again. This is consistent with the interpretation above that qCTC-I is not a purely correlation-induced phase, but instead a mean-field oscillatory phase modified by correlations.

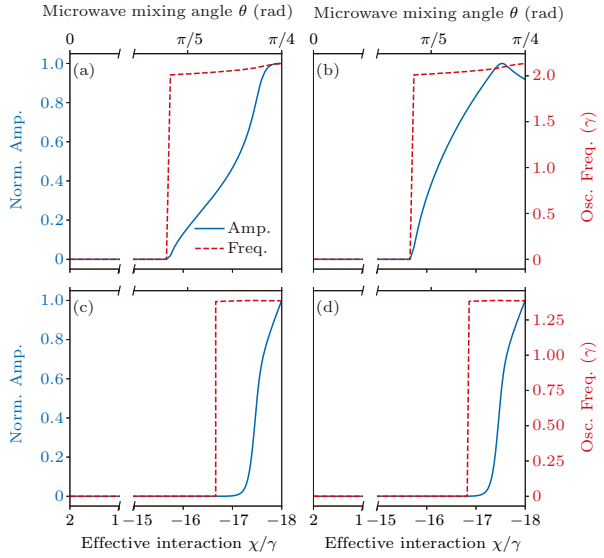


Fig. 5. Scaling of single-particle oscillations and two-body correlations. (a) Oscillation amplitude and frequency of ρ_{++}, and (b) the corresponding nearest-neighbor connected correlator, as functions of the collective interaction strength χ (bottom axis) and microwave mixing angle θ (top axis) in the qCTC-I regime ($\Delta_p = -2.4\gamma, \Omega_p = 2.1\gamma$). In this regime, the onset is associated with a well-defined critical point. (c) and (d) Corresponding quantities in the qCTC-II regime ($\Delta_p = -11.2\gamma, \Omega_p = 8.7\gamma$). In panels (c) and (d), the onset is better interpreted as a smooth crossover rather than a sharp mean-field-like critical transition. The apparent finite jump of the oscillation frequency from zero mainly results from the amplitude threshold 10^{-6} used to identify oscillatory behavior and should not be interpreted as evidence for a true critical point. Other parameters are the same as in Fig. 3.

The behavior of qCTC-II is qualitatively different. Figures 5(c) and 5(d) show that the onset of oscillations is no longer characterized by a well-defined critical point. Instead, the amplitude grows through a smooth crossover, and the nearest-neighbor correlator develops together with the single-particle oscillation amplitude. Within the second-order CME description, this synchronized buildup indicates that the qCTC-II regime is not inherited from a pre-existing mean-field limit cycle. Rather, its oscillatory dynamics are enabled by the same correlations responsible for reshaping the phase diagram in Fig. 3(a). For this reason, qCTC-II is more appropriately interpreted here as a correlation-enabled oscillatory regime rather than a straightforward extension of the classical mean-field continuous-time-crystalline phase.

4. Conclusion

In conclusion, we have proposed a microwave-controlled interaction switch for driven-dissipative Rydberg ensembles. By tuning the microwave dressing, the effective interaction can be continuously reshaped from a short-range form dominated by van der Waals coupling to a longer-range form with an enhanced dipole-exchange contribution. In the mean-field description of thermal gases, this switch drives a supercritical Hopf bifurcation from a steady state to a stable limit cycle, thereby switching the system into dissipative continuous time-crystalline behavior. In two-dimensional lattices, the same switching mechanism remains effective beyond mean-field theory. Spatial correlations reduce the classical oscillatory region while sustaining a correlation-modified oscillatory regime and, within the second-order CME description, additionally enabling a correlation-enabled oscillatory regime absent in mean-field theory. A complementary 2×2 cluster mean-field benchmark yields the same qualitative phase classification, further supporting the robustness of this mechanism beyond mean-field theory. These results establish a direct link between microwave-controlled interaction engineering and nonequilibrium dynamical phases. More broadly, this work shifts the focus from identifying dissipative oscillatory regimes to actively controlling their accessibility through an experimentally tunable interaction parameter.

The parameter regime considered here is compatible with current laser-driven Rydberg platforms. The optical excitation and dissipation assumed in our model correspond to standard driven Rydberg schemes, while the key additional ingredient is microwave control of the effective interaction. This can be realized by coupling an optically excited $|nS\rangle$ Rydberg state to a nearby opposite-parity $|nP\rangle$ state, following established microwave-control schemes for Rydberg interactions.[28] In particular, the representative case $\theta = \pi/4$ used in our calculations corresponds to resonant microwave coupling between the two Rydberg states, whereas other mixing angles can be accessed by adjusting the microwave Rabi frequency and detuning. In this way, the effective interaction can be tuned from a vdW-dominated form toward one with an enhanced dipole-exchange contribution, providing the experimentally accessible interaction switch considered here. The proposed mechanism therefore provides a unified route to controlling dissipative oscillatory behavior from thermal Rydberg gases to 2D lattices and may further facilitate the design of practical nonequilibrium quantum optics devices.

Appendix A: Effective model and cluster mean-field benchmark

In this Appendix, we provide two supplementary results that support the main text. In Section A1, we briefly derive the effective three-level Hamiltonian and the corresponding microwave-controlled interaction $U(R_{ij},\theta)$ starting from the underlying four-level Rydberg scheme. In Section A2, we present a complementary 2×2 cluster mean-field benchmark for representative points in the correlated lattice regime, in order to compare with the cumulant-expansion results and further support the qualitative phase classification discussed in the main text.

A1. Effective three-level Hamiltonian and microwave-controlled interaction

We briefly summarize the derivation of the effective three-level model used in the main text. Starting from a four-level atom with states $|g\rangle$, $|e\rangle$, $|r_1\rangle$, and $|r_2\rangle$, where $|r_1\rangle$ and $|r_2\rangle$ are nearby Rydberg states with opposite parities, the single-atom Hamiltonian within the rotating-wave approximation is

$$\begin{aligned}\hat{H}_{\rm bare} &= \Delta_{\rm p}|g\rangle\langle g| - \Delta_{\rm c}|r_1\rangle\langle r_1| - (\Delta_{\rm c}+\Delta_{\rm m})|r_2\rangle\langle r_2| \\ &\quad + \left(\Omega_{\rm p}|e\rangle\langle g| + \Omega_{\rm c}|r_1\rangle\langle e| + \Omega_{\rm m}|r_2\rangle\langle r_1| + {\rm H.c.}\right). \end{aligned} \tag{A1}$$

Restricting to the Rydberg subspace $\{|r_1\rangle,|r_2\rangle\}$ and diagonalizing the microwave coupling yields the dressed states

$$\begin{aligned}|+\rangle &= \cos\theta|r_1\rangle + \sin\theta|r_2\rangle, \\ |-\rangle &= -\sin\theta|r_1\rangle + \cos\theta|r_2\rangle, \end{aligned} \tag{A2}$$

with $\tan(2\theta) = \frac{2\Omega_{\rm m}}{\Delta_{\rm m}}$, and Autler–Townes splitting $\Delta_{\rm AT} = \sqrt{\Delta_{\rm m}^2+4\Omega_{\rm m}^2}$.

In the dressed basis, the control field couples $|e\rangle$ to both $|+\rangle$ and $|-\rangle$ with amplitudes $\Omega_{\rm c}\cos\theta$ and $-\Omega_{\rm c}\sin\theta$, respectively. Choosing the control-laser detuning such that the $|e\rangle \leftrightarrow |+\rangle$ transition is resonant, the $|e\rangle \leftrightarrow |-\rangle$ transition is detuned by approximately $\Delta_{\rm AT}$. When $\Delta_{\rm AT} \gg \Omega_{\rm c}\sin\theta, \Omega_{\rm p}, \gamma$, the state $|-\rangle$ can be adiabatically eliminated, reducing the system to the effective ladder $\{|g\rangle,|e\rangle,|+\rangle\}$ with coherent Hamiltonian

$$\begin{aligned}\hat{H}_{\rm single} &= \Delta_{\rm p}|g\rangle\langle g| + \Omega_{\rm p}\left(|e\rangle\langle g| + |g\rangle\langle e|\right) \\ &\quad + \Omega_{\rm c}^{(\rm eff)}\left(|+\rangle\langle e| + |e\rangle\langle +|\right), \end{aligned} \tag{A3}$$

where $\Omega_{\rm c}^{(\rm eff)} = \Omega_{\rm c}\cos\theta$. As in the main text, this factor is absorbed into a redefined effective coupling $\Omega_{\rm c}$ by synchronously adjusting the bare control-laser intensity as θ is varied.

The corresponding microwave-controlled interaction is obtained by projecting the two-atom interaction Hamiltonian in the bare basis

$$\begin{aligned}\hat{H}_{\rm int}^{(ij)} &= V_{11}(R_{ij})|r_1r_1\rangle\langle r_1r_1| + V_{22}(R_{ij})|r_2r_2\rangle\langle r_2r_2| \\ &\quad + V_{12}(R_{ij})\left(|r_1r_2\rangle\langle r_2r_1| + |r_2r_1\rangle\langle r_1r_2|\right), \end{aligned} \tag{A4}$$

onto the dressed state $|++\rangle = |+\rangle_i \otimes |+\rangle_j$, which gives

$$\begin{aligned}U(R_{ij},\theta) &= \langle ++|\hat{H}_{\rm int}|++\rangle \\ &= \cos^4\theta\, V_{11}(R_{ij}) + \sin^4\theta\, V_{22}(R_{ij}) \\ &\quad + 2\cos^2\theta\sin^2\theta\, V_{12}(R_{ij}). \end{aligned} \tag{A5}$$

For nearby Rydberg states with similar principal quantum numbers, we take $V_{11}(R_{ij}) \approx V_{22}(R_{ij})$, so that

$$U(R_{ij},\theta) = V_{11}(R_{ij}) + \frac{1}{2}\sin^2(2\theta)\left(V_{12}(R_{ij}) - V_{11}(R_{ij})\right). \tag{A6}$$

This expression shows that the microwave mixing angle θ continuously reshapes the effective interaction from a vdW-dominated short-range form to a longer-range form with an enhanced dipole-exchange contribution.

A2. The 2×2 cluster mean-field benchmark

To complement the second-order cumulant-expansion analysis in the main text, we further perform a 2×2 cluster mean-field (CMF)[44] calculation for representative parameter points in the correlated lattice regime. In this approach, the lattice is partitioned into identical 2×2 plaquettes. Quantum correlations are treated exactly within each cluster, while the inter-cluster coupling is approximated at the mean-field level. The CMF calculation therefore provides an independent benchmark that retains short-range correlations beyond single-site mean field and is complementary to the CME treatment, which captures two-body correlations over the full lattice. Explicitly, we factorize the many-body density matrix into identical 2×2 cluster density matrices, $\hat{\rho} \approx \bigotimes_C \hat{\rho}_C$, and solve the Lindblad dynamics of each cluster self-consistently in the presence of mean fields generated by neighboring clusters.

Here we focus on the same four parameter points used in Fig. 3 of the main text, namely: the qCTC-II point ($\Delta_{\rm p} = -11.2\gamma, \Omega_{\rm p} = 8.7\gamma$), the stationary point ($\Delta_{\rm p} = -6.0\gamma, \Omega_{\rm p} = 8.0\gamma$), the qCTC-I point ($\Delta_{\rm p} = -2.4\gamma, \Omega_{\rm p} = 2.1\gamma$), and the point inside the mean-field oscillatory region but outside qCTC-I ($\Delta_{\rm p} = -1.0\gamma, \Omega_{\rm p} = 2.1\gamma$). For all cases, we consider the microwave-on case with $\theta = \pi/4$ and plot the long-time evolution of the dressed-state population ρ_{++}.

The CMF results are summarized in Fig. A1. At the qCTC-I and qCTC-II points, the late-time CMF dynamics display persistent oscillations of ρ_{++}, in qualitative agreement with the CME results in the main text. By contrast, at the reference stationary point, the CMF trajectory relaxes to a time-independent value, again consistent with the CME prediction. Importantly, for the parameter point that lies inside the single-site mean-field oscillatory region but outside qCTC-I, the CMF dynamics also relax to a steady state rather than sustaining a limit cycle. Taken together, these results show

that the 2×2 CMF calculation reproduces the same qualitative phase classification as the CME analysis: correlations suppress part of the classical oscillatory region, while also supporting an additional oscillatory regime beyond the mean-field theory. This agreement indicates that the main correlation effects discussed in the text are not specific to the CME treatment alone.

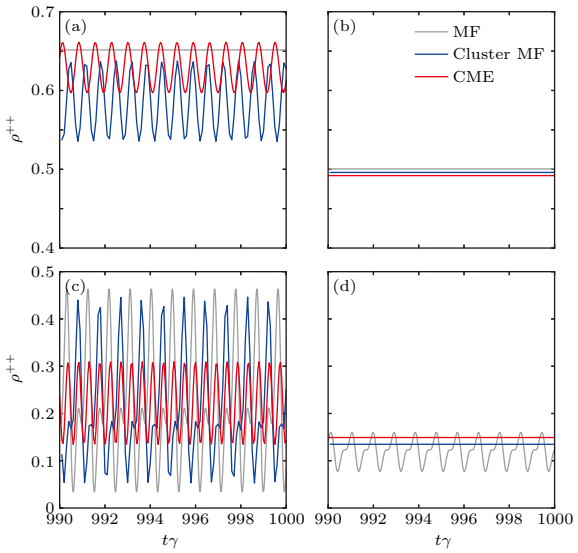


Fig. A1. Late-time evolution of the dressed-state population ρ_{++} for four representative parameter points in the correlated lattice regime, comparing the mean-field, 2×2 cluster mean-field, and CME results. All curves correspond to the microwave-on case with $\theta = \pi/4$ and are shown in the late-time window $990 \leq t\gamma \leq 1000$. Parameters in panels (a)–(d) are identical to those in Figs. 3(b)–3(e), respectively.

Acknowledgments

Project supported by the National Natural Science Foundation of China (Grant No. T2495255). The numerical simulations involved in this paper are performed on the supercomputer provided by Core Facility of Wuhan University.

References

[1] Strocchi F 2021 *Symmetry Breaking* Theoretical and Mathematical Physics (Berlin, Heidelberg: Springer)
[2] Wilczek F 2012 *Phys. Rev. Lett.* **109** 160401
[3] Shapere A and Wilczek F 2012 *Phys. Rev. Lett.* **109** 160402
[4] Bruno P 2013 *Phys. Rev. Lett.* **111** 070402
[5] Watanabe H and Oshikawa M 2015 *Phys. Rev. Lett.* **114** 251603
[6] Kongkhambut P, Skulte J, Mathey L, Cosme J G, Hemmerich A and Keßler H 2022 *Science* **377** 670
[7] Huang Y, Wang T, Yin H, Jiang M, Luo Z and Peng X 2025 *Nat. Commun.* **16** 9375
[8] Iemini F, Russomanno A, Keeling J, Schirò M, Dalmonte M and Fazio R 2018 *Phys. Rev. Lett.* **121** 035301
[9] Gallagher T F 2023 *Rydberg Atoms* in *Springer Handbook of Atomic, Molecular, and Optical Physics* ed Drake G W F (Cham: Springer International Publishing) pp. 231–240
[10] Saffman M, Walker T G and Mølmer K 2010 *Rev. Mod. Phys.* **82** 2313
[11] Malossi N, Valado M M, Scotto S, Huillery P, Pillet P, Ciampini D, Arimondo E and Morsch O 2014 *Phys. Rev. Lett.* **113** 023006
[12] Ding D S, Busche H, Shi B S, Guo G C and Adams C S 2020 *Phys. Rev. X* **10** 021023
[13] Carr C, Ritter R, Wade C G, Adams C S and Weatherill K J 2013 *Phys. Rev. Lett.* **111** 113901
[14] Lee T E, Häffner H and Cross M C 2011 *Phys. Rev. A* **84** 031402
[15] Hu A, Lee T E and Clark C W 2013 *Phys. Rev. A* **88** 053627
[16] He Y, Bai Z, Jiao Y, Zhao J and Li W 2022 *Phys. Rev. A* **106** 063319
[17] Letscher F, Thomas O, Niederprüm T, Fleischhauer M and Ott H 2017 *Phys. Rev. X* **7** 021020
[18] de Melo N R, Wade C G, Šibalić N, Kondo J M, Adams C S and Weatherill K J 2016 *Phys. Rev. A* **93** 063863
[19] Šibalić N, Wade C G, Adams C S, Weatherill K J and Pohl T 2016 *Phys. Rev. A* **94** 011401
[20] Wadenpfuhl K and Adams C S 2023 *Phys. Rev. Lett.* **131** 143002
[21] Wu X, Wang Z, Yang F, Gao R, Liang C, Tey M K, Li X, Pohl T and You L 2024 *Nat. Phys.* **20** 1389
[22] Ding D, Bai Z, Liu Z, Shi B, Guo G, Li W and Adams C S 2024 *Science Advances* **10** eadl5893
[23] Liu B, Zhang L H, Ma Y, Wang Q F, Han T Y, Zhang J, Zhang Z Y, Shao S Y, Li Q, Chen H C, Guo G C, Ding D S and Shi B S 2025 *Nat. Commun.* **16** 1419
[24] Russo F and Pohl T 2025 *Phys. Rev. Lett.* **135** 110404
[25] Xue Y and Bai Z 2026 *Chin. Phys. Lett.* **43** 010302
[26] Yuan J, Yang W, Jing M, Zhang H, Jiao Y, Li W, Zhang L, Xiao L and Jia S 2023 *Rep. Prog. Phys.* **86** 106001
[27] Yuan J, Niu F, Zhang H, Wu C, Chen G, Wang L, Xiao L and Jia S 2026 *Light Manip. Appl.* **1** 202503
[28] Sevinçli S and Pohl T 2014 *New J. Phys.* **16** 123036
[29] Brekke E, Day J O and Walker T G 2012 *Phys. Rev. A* **86** 033406
[30] Buchemmavari V, Omanakuttan S, Jau Y Y and Deutsch I 2024 *Phys. Rev. A* **109** 012615
[31] Qian J 2017 *Sci. Rep.* **7** 12952
[32] Kurdak D, Banner P R, Li Y, Muleady S R, Gorshkov A V, Rolston S L and Porto J V 2025 *Phys. Rev. Lett.* **134** 123404
[33] Strogatz S H 2024 *Nonlinear Dynamics and Chaos : With Applications to Physics, Biology, Chemistry, and Engineering* 3rd ed (New York: Chapman and Hall/CRC)
[34] Cohen-Tannoudji C, Diu B and Laloë F 2019 *Quantum Mechanics, Volume 3: Fermions, Bosons, Photons, Correlations, and Entanglement* (John Wiley & Sons)
[35] Scully M O and Zubairy M S 1997 *Quantum Optics* (Cambridge : Cambridge University Press)
[36] Diehl S, Tomadin A, Micheli A, Fazio R and Zoller P 2010 *Phys. Rev. Lett.* **105** 015702
[37] Tomadin A, Diehl S and Zoller P 2011 *Phys. Rev. A* **83** 013611
[38] Wang Z, Gao R, Wu X, Buča B, Mølmer K, You L and Yang F 2025 *Phys. Rev. Lett.* **135** 230401
[39] Kubo R 1962 *J. Phy. Soc. Jpn.* **17** 1100
[40] Lackner F, Březinová I, Sato T, Ishikawa K L and Burgdörfer J 2017 *Phys. Rev. A* **95** 033414
[41] Plankensteiner D, Hotter C and Ritsch H 2022 *Quantum* **6** 617
[42] Donsa S, Lackner F, Burgdörfer J, Bonitz M, Kloss B, Rubio A and Březinová I 2023 *Phys. Rev. Res.* **5** 033022
[43] Heeg K P, Gärttner M and Evers J 2012 *Phys. Rev. A* **86** 063421
[44] Jin J, Biella A, Viyuela O, Mazza L, Keeling J, Fazio R and Rossini D 2016 *Phys. Rev. X* **6** 031011